Fermi National Accelerator Laboratory

Hard Diffraction and Rapidity Gaps

A. Brandt

For the D0 Collaboration

Fermi National Accelerator Laboratory
P.O. Box 500, Batavia, Illinois 60510

September 1995

Disclaimer

A Review of Hard Diffraction and Rapidity Gaps [*]

Andrew G. Brandt [†]

The DØ Collaboration

Fermi National Accelerator Laboratory

P.O. Box 500

Batavia, IL 60565

The field of hard diffraction, which studies events with a rapidity gap and a hard scattering, has expanded dramatically recently. A review of new results from CDF, DØ, H1 and ZEUS will be given. These results include diffractive jet production, deep-inelastic scattering in large rapidity gap events, rapidity gaps between high transverse energy jets, and a search for diffractive W-boson production. The combination of these results gives new insight into the exchanged object, believed to be the pomeron. The results are consistent with factorization and with a hard pomeron that contains both quarks and gluons. There is also evidence for the exchange of a strongly interacting color singlet in high momentum transfer ($36 < |t| < 1000$ GeV^2) events.

I. INTRODUCTION

The properties of elastic and diffractive scattering are well-described in the context of Regge theory [1,2] by pomeron exchange, where the pomeron is a color singlet with quantum numbers of the vacuum [3,4]. The exact nature of the pomeron, or whether it even exists, is an open question. The landmark paper of Ingelman and Schlein [5] proposed that the observation of jets in diffractive events would probe the partonic nature of the exchanged object (pomeron). This paper introduced the field of hard diffractive scattering, which refers to the subset of traditional diffractive interactions that have a high transverse momentum (p_T) scattering. They assumed that the pomeron can be treated as an object that exists within a proton, and that it is thus sensible to define a flux of pomerons in the proton as well as a pomeron structure function. They proposed a gluonic pomeron with either a hard structure as would be derived from two gluons sharing the pomeron momentum $\sim \beta(1-\beta)$, or a soft structure like the gluonic structure of the proton $\sim (1-\beta)^5$, where β is the momentum fraction of the parton with respect to the pomeron.

First experimental results on this subject were published by the UA8 Collaboration, which showed the existence of jets in single diffractive events [6] and that these jets had rapidity and longitudinal momentum distributions consistent with a hard pomeron structure [7]. There was also evidence for a "super-hard" or "coherent" pomeron, where the entire momentum of the pomeron participates in the hard scattering [7].

The UA8 Collaboration tagged diffractive events using a small angle spectrometer consisting of Roman pots to detect and reconstruct the leading proton [8]. Diffractive events can also be tagged using rapidity gaps [9,10], which are defined as the absence of particles or energy above threshold in some region of rapidity. Since the pomeron is a color singlet, radiation is suppressed in events with pomeron exchange resulting in large rapidity gaps in these events [11].

In this paper, new results on the subject of hard diffractive scattering and pomeron structure will be reviewed. The paper is divided into two main subjects:

- Pomeron structure, which includes hard diffractive scattering results from HERA and the Tevatron as well as deep-inelastic scattering (DIS) in diffractive events. These processes are dominated by low momentum transfer $(t \sim 0)$ exchange.

- Rapidity gaps between jets. This subject is concerned with high momentum transfer color-singlet exchange, and is not sensitive to the structure of the exchanged object.

II. POMERON STRUCTURE

A. HERA Diffractive Jet Studies

The observation of large rapidity gaps in DIS events at HERA [9,10] is well-described by traditional diffractive scattering models assuming pomeron exchange. This result is to be

expected in the context of Regge theory and factorization, since pomeron exchange would be expected to be the same in any reaction involving protons, whether it be ep, πp, pp, or $p\bar{p}$. With sufficient statistics, it is possible to search for jet structure in diffractive events, which are tagged by the existence of a large rapidity gap. Experimentally, a large rapidity gap is defined using the variable η_{MAX}, which is the η of the most forward energy deposit above threshold. Typical η_{MAX} values are large ($\eta_{\mathrm{MAX}} \sim 4$) as the proton remnant deposits energy near the beam pipe in the forward calorimeter. Small η_{MAX} values thus indicate the presence of a large rapidity gap.

The Monte Carlo POMPYT [12] incorporates the Ingelman-Schlein model and can be used to compare jets observed in diffractive events to jets produced with different assumptions about the pomeron structure. The Monte Carlo assumes factorization and that the momentum sum rule is satisfied (all of the pomeron's momentum is carried by the partons, as if the pomeron is a particle), and allows for the choice of a pomeron composed of gluons or quarks with hard or soft structure. These assumptions are being tested at HERA and the Tevatron.

Diffractive jet production at HERA was initially observed in DIS events with a large rapidity gap [13]. These jets are well-described by the exchange of a pomeron with hard structure $\sim \beta(1 - \beta)$, as expected from the UA8 results. Recently, more extensive analysis has been done with jets produced in photoproduction (where a quasi-real $Q^2 \approx 0$ photon is exchanged) events with a large rapidity gap [14,15].
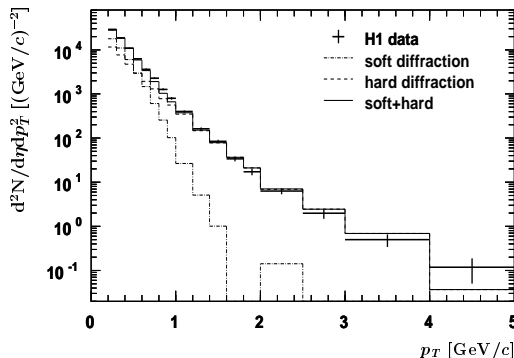

FIG. 1. Transverse momentum distribution of charged particles for events with $\eta_{\mathrm{MAX}} < 1.5$ compared to Monte Carlo predictions for soft and hard diffraction.

Signatures of hard scattering in photoproduction events include a large p_T tail in the inclusive single particle distribution, and an increase in the azimuthal back-to-back correlation of the transverse energy flow with increasing event E_T [15]. In Fig. 1, the H1 Collaboration shows the single particle p_T distribution for data compared to Monte Carlo predictions. The p_T for charged tracks with $|\eta| < 1.5$ is measured with respect to the beam axis, where POMPYT is used for hard diffraction and is normalized to the region $p_T > 1.5$ GeV/c. The data have a much harder p_T spectrum than that predicted by a PYTHIA Monte Carlo [16] standard diffractive process (dash-dotted histogram), but a combination of soft and hard diffraction (solid histogram) gives a good representation of the data.

3

Thrust $T_\perp = \max(\Sigma \mathbf{p}_T \cdot \mathbf{n}/\Sigma |\mathbf{p}_T|)$ is a variable sensitive to event shape, where p_T is the transverse momentum vector for charged tracks and calorimeter clusters, and n is the unit vector which maximizes $T_\perp$. For a two-body decay $T_\perp = 1$, and in the infinite multiplicity isotropic limit it approaches 0.64. Figure 2 shows the mean thrust versus event E_T for data compared with the expectation for an isotropic system. The average thrust decreases with E_T until about 9 GeV where it increases showing a clear two-body structure. Note that this result is model independent.
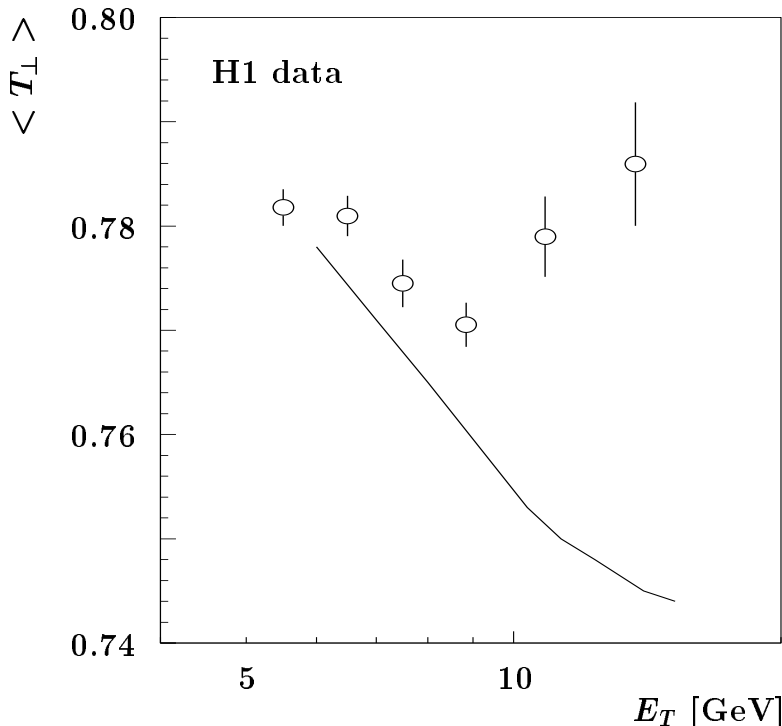

FIG. 2. Average observed transverse thrust as a function of event E_T. The line shows the expectation for azimuthally isotropic events with the same average multiplicity as the data points.

The ZEUS Collaboration shows event characteristics from a sample of photoproduction events with at least one jet with $E_T > 6$ GeV and $|\eta| < 1$ [17]. Figure 3(a) shows $M_X^{\mathrm{CAL}} = \sqrt{E^2 - \vec{p}^2}$ (the mass of the diffractive system as measured in the calorimeter) versus η_{MAX} for all jet events. A group of events with $M_X^{\mathrm{CAL}} < 30$ GeV and $\eta_{\mathrm{MAX}} < 1.8$ is observed outside of the central cluster of events. In Fig. 3(b), the η_{MAX} distribution is shown for this M_X^{CAL} bin and it is obvious that PYTHIA alone is insufficient to describe the data. The POMPYT Monte Carlo with hard gluon structure normalized for $\eta_{\mathrm{MAX}} < 2.5$ gives a good description of the large rapidity gap events. The M_X^{CAL} distribution for events with $\eta_{\mathrm{MAX}} < 1.8$ is shown in Fig. 3(c), and is also well-modelled by POMPYT. Figure 3(d) shows that W^{CAL} (the center-of-mass energy of the $\gamma^* p$ system) for the large rapidity gap events is again modelled well by POMPYT. Note that the hard gluonic pomeron structure is used for the Monte Carlo, but there is little sensitivity between hard and soft or gluons and quarks in these distributions, although a hard structure is marginally preferred in the η_{MAX} distribution.
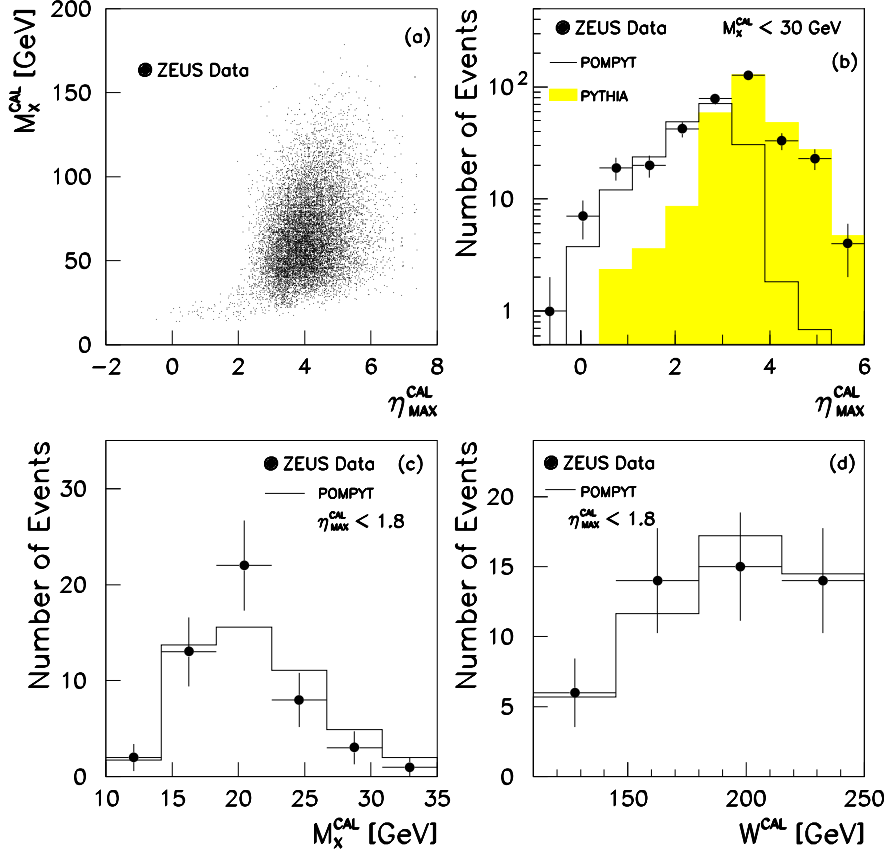
FIG. 3. (a)Scatter plot of M_X^{CAL} versus η_{MAX} for inclusive jet events. (b) The η_{MAX}distribution for events with $M_X^{CAL} < 30$ GeV. The shaded region is the PYTHIA prediction and the solid line gives the POMPYT hard gluon prediction. The Monte Carlos are normalized to the number of events above (PYTHIA) and below (POMPYT) $\eta_{MAX} = 2.5$. (c) and (d) show the M_X^{CAL} and W^{CAL} distributions, respectively, for $\eta_{MAX} < 1.8$ along with the POMPYT prediction.

In Fig. 4 [17], the ZEUS Collaboration shows the inclusive jet cross section for events with $\eta_{MAX} < 1.8$. A cone algorithm with radius $R = \sqrt{\Delta\eta^2 + \Delta\phi^2} < 1$ is used and the jet E_T threshold is 8 GeV. The inner statistical error bars show the dominant error ($\sim 30\%$) in the measurement and the shaded region shows the energy scale uncertainty ($\sim 20\%$). The PYTHIA non-diffractive prediction (dashed curve) shows that it is possible to get large rapidity gaps from fluctuations, but has a different shape and is seen to be well below the data by an η-dependent factor of between 2 and 7. Different pomeron structure assumptions are also shown, with the best agreement given by the hard gluon ($6\beta(1-\beta)$) structure. The hard quark ($(6/4)\beta(1-\beta)$) gives a similar shape but is 3–10 times below the data. The soft gluon ($6(1-\beta)^5$) disagrees dramatically, both in shape and normalization. Note that all Monte Carlo predictions use the same jet algorithm as the data, performed at the hadron level, and the structure function coefficients are obtained using the momentum sum rule.
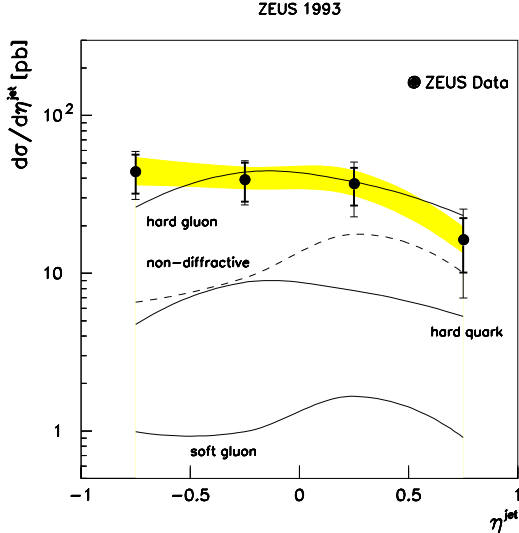
FIG. 4. The measured differential ep cross section $d\sigma/d\eta^{jet}$ for inclusive jet production for $E_T > 8$ GeV, $Q^2 < 4$ GeV^2, and $\eta_{\mathrm{MAX}} < 1.8$. The measurements are not corrected for non-diffractive and double dissociation processes. The inner error bars are statistical, and the total error bars show statistical and systematic errors, excluding the energy scale errors shown by the shaded band. The dashed curve shows the non–diffractive contribution, while the solid curves show the POMPYT prediction for different assumed pomeron structures.

B. HERA Deep-Inelastic Scattering in Large Rapidity Gap Events

Deep-inelastic electron-proton scattering (DIS) uses a virtual boson to probe the structure function F_2 of the proton [18,19]. The sample of DIS events that have a large rapidity gap are dominantly diffractive, and hypothesized to be due to the exchange of a colorless component of the proton, the pomeron ($\mathbb{P}$). Under this assumption, it is possible to measure the "diffractive structure function" F_2^D [20,21]. This quantity is derived from the DIS cross section (see [20,21] for further details) and is a function of $x_{\mathbb{P}}$, the momentum fraction of the exchanged pomeron, β, the momentum fraction of the struck quark with respect to $x_{\mathbb{P}}$, and Q^2 the negative of the squared four-momentum transfer of the virtual photon. Note that x, the momentum fraction of the parton in the proton typically used in F_2 measurements, is simply related to $x_{\mathbb{P}}$ and β through $x = x_{\mathbb{P}}\beta$. An integral is performed over t, the four-momentum transfer to the proton, since the proton is not measured for this data sample. The measurement of F_2^D allows a test of factorization as shown in the following equation:

$$F_2^D(\beta, Q^2, x_{\mathbb{P}}) = f_{\mathbb{P}}(x_{\mathbb{P}}) \cdot F_2^{\mathbb{P}}(\beta, Q^2)$$

where $f_{\mathbb{P}}(x_{\mathbb{P}})$ is the flux of pomerons in the proton, and $F_2^{\mathbb{P}}(\beta, Q^2)$ is the pomeron structure function independent of the emission of the pomeron.

Figure 5 shows F_2^D as a function of $x_{\mathbb{P}}$ for several bins of β and Q^2 from the H1 Collaboration. The fit shown is $(x_{\mathbb{P}})^{-n}$ where $n = 1.19 \pm 0.06$ $(stat) \pm 0.07(sys)$. A similar

6

measurement from ZEUS gives $n = 1.30 \pm 0.08 \ (stat) \ ^{+ \ 0.08}_{- \ 0.14} \ (sys)$. The excellent fit in all bins gives strong evidence for factorization. The expectation from Regge theory is $(x_{I\!P})^{-(2\alpha(t)-1)}$, where $\alpha(t)$ is the pomeron trajectory, and a phenomenological evaluation of this expression at $t = 0$ gives $\alpha = 1.085$ [22]. The measured values of n at HERA give $\alpha \approx 1.1$, and are thus completely consistent with the pomeron trajectory and inconsistent with other leading meson trajectories or pion exchange.
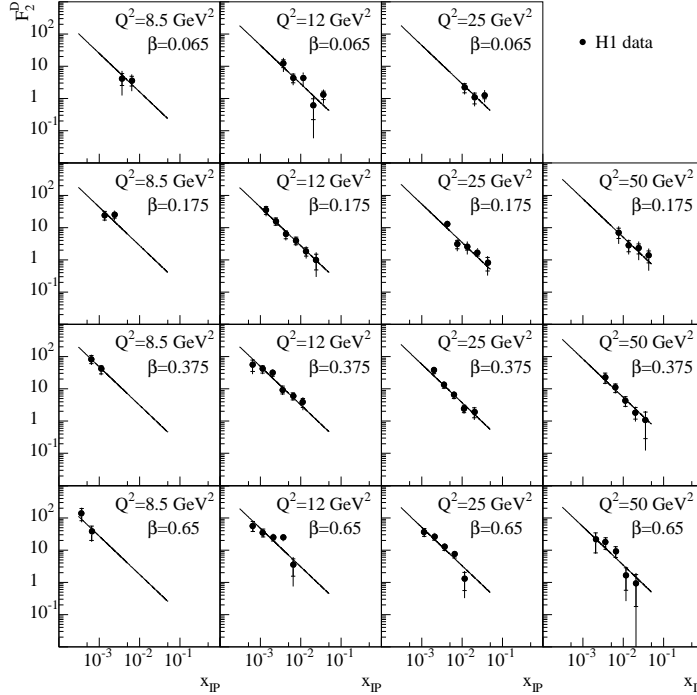

FIG. 5. F_2^D, the diffractive component of F_2, is shown as a function of $x_{I\!P}$ for various bins of β and Q^2. The inner error bar shows the statistical error, wile the full error shows the statistical and systematic error added in quadrature. A fit to the form $c(x_{I\!P})^{-n}$ is also shown (see text).

Next an integration over $x_{I\!P}$ is performed allowing the evaluation of F_2^D as a function of β and Q^2. In the second column of Fig. 6 from the ZEUS Collaboration, little Q^2 dependence is observed in fixed β bins implying that the interaction is scale invariant, and thus of a point-like nature, consistent with scattering off quarks in the pomeron. The β dependence in fixed Q^2 bins is also rather flat (first column), indicating that unlike the proton, a large fraction of the pomeron typically interacts. A soft $\sim (1 - \beta)^5$ pomeron is ruled out, and a hard $\sim \beta(1 - \beta)$ (dashed curve) or flat dependence is preferred. The solid line includes a $(1 - \beta)^2$ softer contribution, which combined with the hard distribution gives a good fit to the data. Note that the excess in data with respect to the hard pomeron structure could also conceivably be accounted for by the lack of Q^2 evolution in POMPYT. Due to resolution problems at β values near unity, it is difficult to comment on the possibility of a "super-hard" pomeron, although the H1 Collaboration claims a somewhat better fit to their version of Fig. 6 when a "super-hard" component is included.
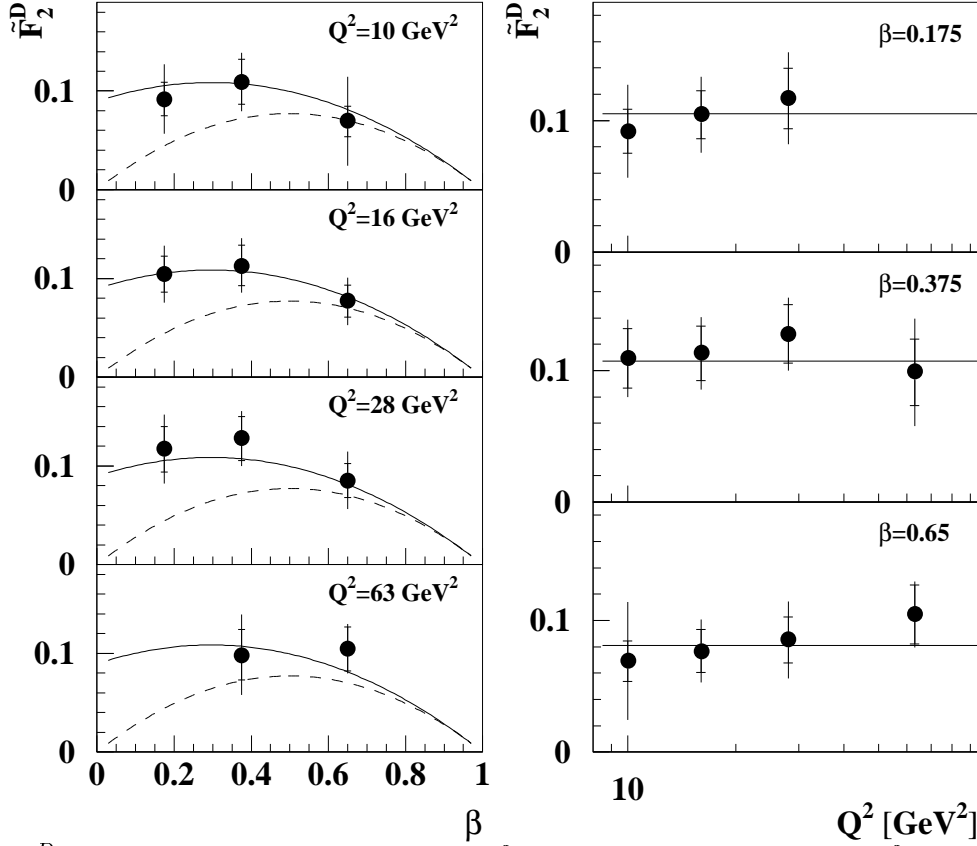
ZEUS 1993

FIG. 6. F_2^D is shown as a function of β in Q^2 bins and as a function of Q^2 in β bins. The inner error bars shows the statistical component of the error. The dashed curve is for a $\sim \beta(1-\beta)$ pomeron structure, while the solid curve also includes a softer component as discussed in the text.

C. HERA Pomeron Structure Conclusions

The jet cross section measurements can be combined with the DIS measurements to give information on the pomeron structure [17]. Assuming that the momentum sum rule ($\Sigma_{I\!P} = 1$) is satisfied, the jet cross section measurements prefer a hard gluon dominated pomeron. The DIS measurements show that there is a hard quark component of the pomeron, but do not favor a structure which simultaneously satisfies the momentum sum rule and is composed exclusively of quarks. ZEUS has combined these two studies and extracted a range for the gluon content of the pomeron [17].

After subtracting the non-diffractive and double dissociation contributions from the jet cross section, the data are compared to the POMPYT predictions allowing for a mixture of hard gluon ($6\beta(1-\beta)$) and hard quark ($(6/4)\beta(1-\beta)$) densities, with the fraction of gluons (c_g) and the overall normalization ($\Sigma_{I\!P}$) left as free parameters. For each value of c_g, a χ^2 fit to the data was performed, as shown by the solid line in Fig. 7, with the shaded band showing the 1σ uncertainty.
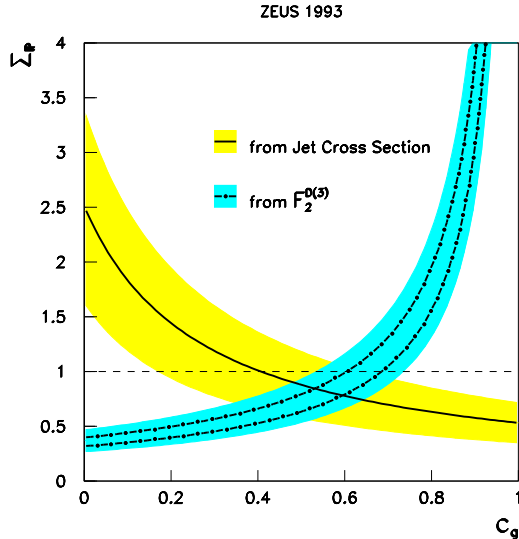
FIG. 7. The plane of variables $\Sigma_{I\!P}$(momentum sum) and c_g (relative fraction of gluons in the pomeron). The solid line shows the χ^2 fit as a function of c_g from the corrected jet cross section and POMPYT predictions, with the shaded region showing the 1 σ error band. The constraint from the DIS F_2^D measurement is shown as the dot-dashed line for two choices of the number of flavors. The dashed line shows $\Sigma_{I\!P} = 1$.

Assuming that the same pomeron parton densities describe both the DIS and photoproduction data, the DIS results add an additional constraint to this figure. An integral of F_2^D over $x_{I\!P}$ and β is performed giving a value of $\Sigma_{I\!P}$ which is approximately independent of Q^2. This integral gives the constraint $\Sigma_{I\!P} \cdot c_q = 0.32(0.4)$ for two choices of the number of flavors, where c_q is the quark fraction. Using the relation $c_q = 1 - c_g$, this constraint is shown as the dot-dashed curves in Fig. 7. The intersection of the two curves gives a range of $0.5 < \Sigma_{I\!P} < 1.1$ and $0.35 < c_g < 0.7$, not including systematic errors. Several uncertainties are noted about this approach, including the leading order nature of the Monte Carlo calculations, the model dependence of the background subtraction, the factorization assumption, and flux factor dependence. Taking these errors into account gives $0.3 < c_g < 0.8$ and $0.4 < \Sigma_{I\!P} < 1.6$, where c_g is independent of flux factor variation, but $\Sigma_{I\!P}$ could vary by an additional 30%. This analysis indicates that the pomeron has a significant hard gluon component and is consistent with the momentum sum rule.

D. Tevatron Diffractive W-Boson Production

A compelling way to probe the pomeron structure at the Tevatron is by searching for diffractively produced W-bosons [23]. The quark component of the pomeron can be tested through the leading order process $q\bar{q} \rightarrow W$, while the gluon component is suppressed by α_s and would produce W's via $gq \rightarrow Wq$. The fraction of $W \rightarrow l\nu$ cross section that is diffractive has been predicted to be 17% for a hard-quark pomeron and 0.8% for a hard-gluon pomeron assuming a momentum sum rule and standard pomeron flux [23].

The experimental search makes use of the diffractive event topology, in which the lepton is more likely to be produced in the hemisphere opposite the rapidity gap. For non-diffractive production, any rapidity gaps would be due to multiplicity fluctuations and there is no correlation expected between the location of the lepton and the rapidity gap. The CDF calorimeter [24] is used to search for rapidity gaps. The multiplicity of towers with $E_T > 200$ MeV is measured in the pseudorapidity region $2 < \eta < 4.2$, where the tower size is $0.1 \times 5°$ in $\Delta \eta \times \Delta \phi$. Standard W-selection requirements are applied, in addition, events with more than one vertex have been removed since multiple interactions could spoil rapidity gaps.

The resulting multiplicity distribution is shown in Fig. 8 [25]. The solid(dashed) histogram shows the multiplicity in the opposite(same) hemisphere of the lepton. Although more than 5% of the events have a rapidity gap (no towers above threshold), there is no clear excess of rapidity gaps (zero multiplicity) in the opposite side sample as expected from diffractive W's. The bottom part of this figure shows that the difference of the two histograms divided by the sum is consistent with zero over the whole range of multiplicities.

A similar but independent asymmetry analysis can be applied using the fact that a proton (with two u quarks and one d quark) is about twice as likely to produce a W^+ $(u\bar{d})$ as a W^- $(d\bar{u})$, when interacting with a $\mathbb{P}$ $(q\bar{q})$. Therefore, rapidity gaps in diffractive $W^+(W^-)$ events are expected to occur preferentially in the $\bar{p}(p)$ direction. Fig. 9 shows the charge asymmetry multiplicity results in a manner similar to the topology results. Again no clear excess is observed at zero multiplicity.
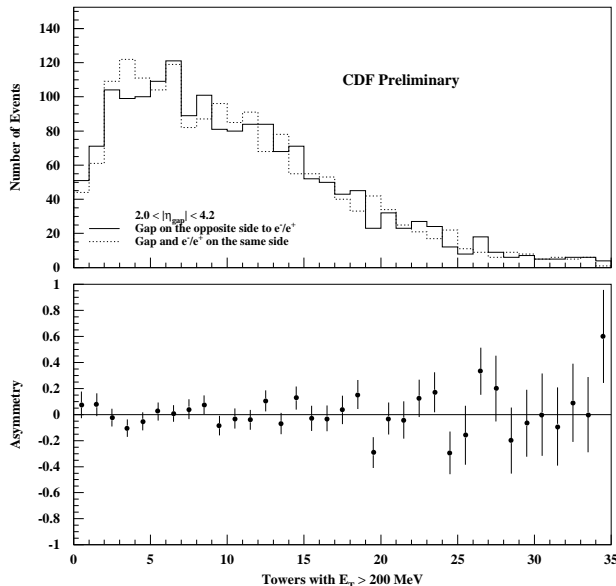

FIG. 8. Multiplicity distribution of towers with $E_T > 200$ MeV in the region $2.0 < |\eta| < 4.2$ on the opposite side (solid histogram) of the central lepton ($|\eta| < 1.1$) and on the same side (dashed histogram). The bottom plot shows the difference between the solid and dashed histograms divided by the sum.
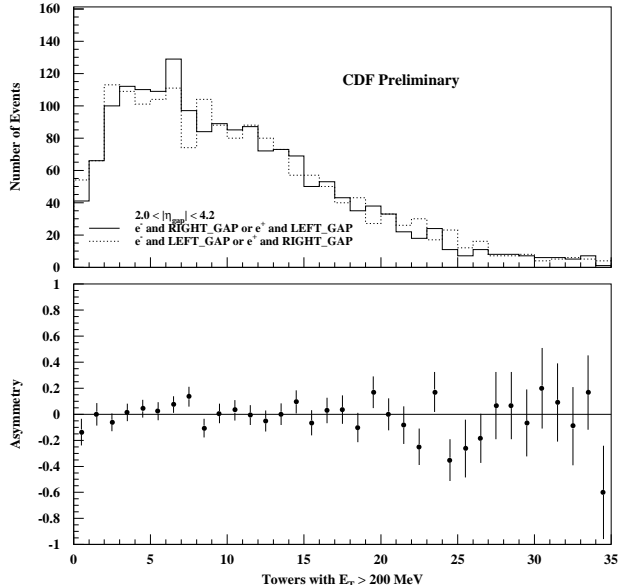
FIG. 9. Charge asymmetry version of Fig. 8, with the solid histogram showing the charge correlated with the side of the rapidity gap and the dashed histogram the anti-correlation of charge with the side of the rapidity gap. The bottom plot again shows the difference between the solid and dashed histograms divided by the sum.

The fraction of W events that could be attributed to diffraction is measured from the asymmetries to be $0.2 \pm 0.8\%$. After correcting for noise effects and combining the results with a Monte Carlo study of how often a diffractive event yields a rapidity gap, a preliminary limit on the diffractive component of W's as less than a few per cent (the systematics are still under study) is obtained. This is clearly less than the fully normalized quark pomeron prediction and can be used to place a limit on the quark component of the pomeron.

E. Tevatron Diffractive Jet Production

CDF also has a sample of jet events taken with a special trigger demanding that 2 jets have $E_T > 20$ GeV and $\eta > 1.8$ [25]. This yields a sample after cuts of about 1000 events with jets on opposite sides (OS) of the detector in rapidity, and 3400 same side (SS) jet events. The same side jet sample is an ideal place to search for hard diffractive scattering, where a rapidity gap is typically expected to occur in the hemisphere opposite the jets. The prediction from POMPYT for a fully normalized hard gluonic pomeron is that 5.3% of events are expected to be due to diffractive scattering. As in the W case, multiple interaction events are rejected and the multiplicity in the region $2 < \eta < 4.2$ (opposite the jets) is plotted. Figure 10 shows the tower multiplicity for same side jet events (solid histogram) and central lepton W events (dashed histogram). Two entries are made for each W event ($+\eta$ and $-\eta$), central muon events are used as well as electron events, and the W sample is normalized

11

to the same side sample for $n_{tower} > 0$. Again a small fraction ($2.9 \pm 0.3\%$) of events have a rapidity gap, but compared to the W multiplicity distribution, no excess is seen. The fraction of diffractive events is corrected for noise (which is found to ruin 13% of rapidity gap events) and the efficiency for Monte Carlo diffractive events to give a rapidity gap (94%), resulting in a fraction of $-0.4 \pm 0.5\%$. This is used to place an upper limit of 0.4% (95% CL) on the fraction of jet events attributable to diffraction, assuming that there is no diffractive W production [25].

CDF Preliminary

Tower Multiplicity Distribution
η Range 2.0 - 4.2

— **Same Side Jets (3415 Events)**
- - - **Central Electron+Muon W**
2(1734+1275) W Entries
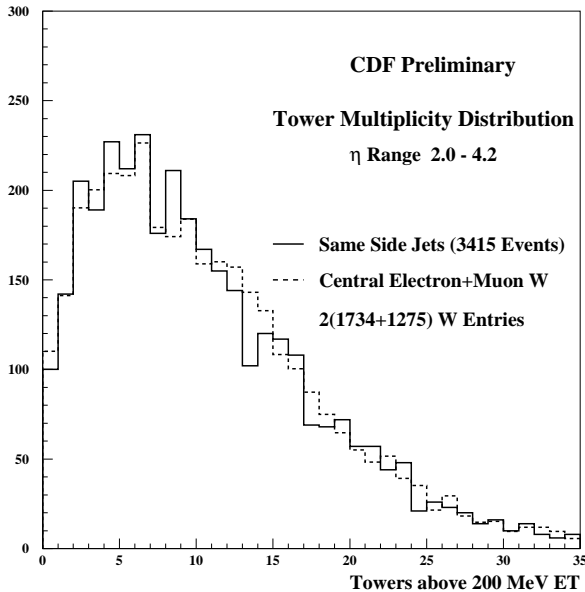
Towers above 200 MeV ET

FIG. 10. Multiplicity distribution of towers with $E_T > 200$ MeV in the region $2.0 < |\eta| < 4.2$ on the side opposite the same side jets (solid histogram) compared to the equivalent region for central lepton W events. The W sample is normalized to the SS sample for $n_{tower} > 0$.

F. Pomeron Structure Conclusions

The ZEUS and H1 Collaborations have made major strides in understanding the nature of the pomeron. The recent measurement of jet cross sections are consistent with pomeron exchange, and, combined with the DIS measurements, imply that the pomeron is dominantly hard and composed of both quarks and gluons. New data including Roman pot spectrometers to measure the proton momentum are anticipated soon and will shed more light on the structure of the pomeron.

The CDF Collaboration has new measurements putting limits on diffractive W and jet production, which in turn put limits on the partonic structure of the pomeron. More data are available in the current run and it should be possible to establish if the pomeron is behaving consistently in ep and $p\bar{p}$ interactions. DØ has specialized triggers in the current run, including these two subjects as well as double pomeron exchange, which may be a good

place to look for the "super-hard" pomeron.

III. RAPIDITY GAPS BETWEEN JETS

A. Introduction

Rapidity gaps are expected to occur between jets when a color-singlet is exchanged between the interacting hard partons [26]. The exchange of a photon [27], W-boson, Z-boson or a hard QCD pomeron [28,11] is expected to give such an event topology. Although the cross section for electroweak gauge boson exchange is small, the cross section for two-gluon pomeron exchange is believed to be significant [28,29], and roughly 10% of jet events may be due to pomeron exchange [28]. Typical color-exchange jet events (single gluon or quark exchange) have particles between jets, but rapidity gaps can arise from fluctuations in the particle multiplicity, which is expected to have a negative binomial or similar distribution [30]. These "background" rapidity gap events become highly suppressed as the jet rapidity separation is increased.

Rapidity gaps will not be observed in the final state, however, if spectator interactions produce particles between the jets. Approximately 10–30% of rapidity gap events are expected to survive spectator interactions [28,31]. Thus roughly 1–3% of jet events are expected to have an observable rapidity gap between the jets from pomeron exchange.

Although it is not possible to distinguish color-singlet rapidity gaps from those that occur in color-octet (gluon) exchange on an event-by-event basis, differences in the expected particle multiplicity distributions can be used to search for a color-singlet signal. This signal is expected to appear as an excess of events at low particle multiplicity compared to the negative binomial-like distribution expected for color-octet exchange.

Experimentally both DØ and CDF measure the multiplicity of particles in the pseudo-rapidity interval ($\Delta\eta_c = |\eta_1 - \eta_2| - 2\mathcal{R}$) between the cone edges ($\mathcal{R} = \sqrt{\Delta\eta^2 + \Delta\phi^2} = 0.7$) of the two highest E_T jets.

The DØ Collaboration has published a study of rapidity gaps between jets [32], using the observation of rapidity gaps with an experimental definition to place an upper limit on the fraction of events with a rapidity gap between the jets (1.1% at 95% CL) [32].

The CDF Collaboration has published [33] the fraction of jet events with a rapidity gap using a smooth fit to the tracking multiplicity distribution to estimate the background from fluctuations. They quote a fraction of $0.0085 \pm 0.0012(stat)^{+0.0012}_{-0.0024}(sys)$.

The new analyses on this subject from CDF, DØ, and ZEUS are described below.

B. CDF Analysis

The data set used in the CDF analysis of rapidity gaps in opposite side (OS) jet events is described in Sec. II E. The particle multiplicity distribution between jets is determined using three dimensional tracks in the Central Tracking Chamber (CTC). Tracks are required

to have transverse momentum (p_T) > 300 MeV, a horizontal displacement from the vertex of less than 8 cm, and an impact parameter of less than 0.8 cm.

In Fig. 11 [25], the track multiplicity is compared for OS jet events in a region $|\eta|$ < 1.1 with SS jets in the region $|\eta|$ < 1.2, where the region size is optimized to match the mean multiplicities for the two samples. The number of SS events has been normalized to the number of OS events excluding the zero multiplicity bin. The SS and OS multiplicities are in good agreement over the entire range except for the zero bin, which has an excess of $21.5 \pm 7.0(stat)$ events in the opposite side sample. This corresponds to a fractional excess of $2.0 \pm 0.7(stat) \times 10^{-2}$. The measurement has been repeated for several different $|\eta|$ ranges and the excess is consistent within statistical errors.
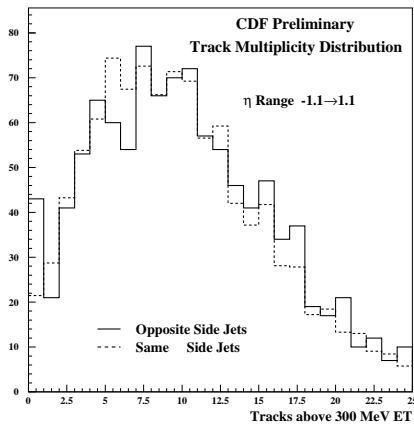

FIG. 11. Track multiplicity distributions for OS ($|\eta|$ < 1.1, mean=9.87 tracks) events and SS ($|\eta|$ < 1.2, mean=9.73) events. The number of SS events has been normalized to the number of OS events excluding the zero–track bin.

To verify that the zero-track events are not caused by a detector effect the correlations between track and calorimeter tower multiplicities were examined. The tower multiplicity is on average higher than the track multiplicity because the calorimeter detects both neutral and charged particles, has a lower energy threshold, and also detects additional particles due to showering outside of the jet cones. The excess is smeared over the first several bins but gives a total excess consistent with the tracking.

C. DØ Analysis

The data sample used in the DØ analysis is derived from a special high-$\Delta\eta_c$ trigger [32] implemented to obtain events with large pseudorapidity separation ($\Delta\eta_c$) between the cone edges of the two highest E_T jets. In the offline analysis, events are required to have at least two jets, each with $E_T > 30\,\text{GeV}$ and $|\eta| > 2$. Events with more than one interaction in a proton-antiproton crossing are removed since they include a source of particles not associated with the triggering interaction. Particles are tagged in the electromagnetic section of the

14

calorimeter [34] by requiring $E_T > 200\,\text{MeV}$ in a calorimeter tower [32], with the number of tagged particles in a given pseudorapidity region denoted by N_{EM}.

The color-octet background is modelled using a negative binomial distribution which gives a reasonable fit to PYTHIA Monte Carlo distributions of particles and towers between jets, both before and after detector simulation. An enriched color-octet sub-sample of the data was also studied. This sample was obtained by requiring a jet ($E_T > 8\,\text{GeV}$) to be in the $\Delta\eta_c$ region between the two leading jets. Figure 12(a) shows the tagged-particle multiplicity distribution between the two highest E_T jets for $\Delta\eta_c > 3$. Another control sample of data consisted of events in which the two leading E_T jets were found on the same side (in rapidity) of the detector. To remove any color-singlet contribution to this sample from hard single diffractive events, a beam-beam coincidence was required (produced by the break up of the proton and anti-proton). Figure 12(b) shows the multiplicity in a region of $\Delta\eta = 2.4$ centered around $\eta = 0$ for these events. Both distributions are consistent with a negative binomial distribution which demonstrates that detector effects do not produce an excess of events at low multiplicities and that a negative binomial distribution describes these color-exchange samples.
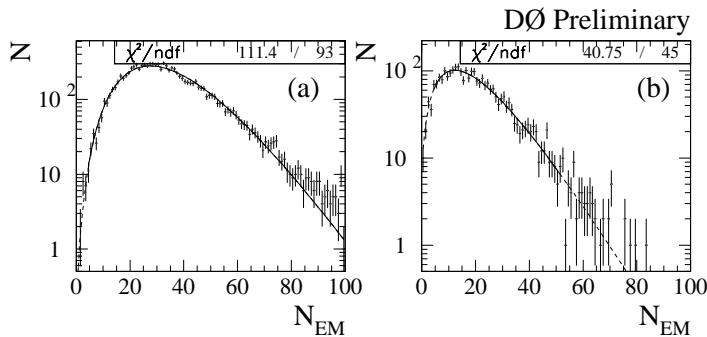

FIG. 12. The preliminary tagged–particle multiplicity distributions obtained from color–octet events for (a) the data sample where a jet is required to be in the region $\Delta\eta_c$ (b) a sample of events where both jets are on the same side of $\Delta\eta$. Negative binomial fits to the data (solid lines) are also shown.

The inclusive tagged-particle multiplicity distribution for events with $\Delta\eta_c > 3$ is shown in Fig. 13, with the bottom figure showing the same quantity on a log-log scale. A significant excess is observed at small particle multiplicity, $N_{\text{EM}} < 4$, compared to a negative binomial (dashed curve) and double negative binomial fit (solid curve). The preliminary excess is $263 \pm 21(stat) \pm 10(sys)$ events for the single negative binomial and $154 \pm 21(stat) \pm 16(sys)$ for the double negative binomial, where the systematic error currently only includes the error on the fit parameters. The starting bin of the fit of $N_{\text{EM}} = 4$ has been chosen to minimize the resulting χ^2. Although both distributions give a $\chi^2 \approx 1$, shape tests show systematic differences between the single negative binomial and the data. The double negative binomial (sum of two negative binomials), which has a better shape agreement and a somewhat smaller excess, is thus introduced. Monte Carlo studies show that the double negative binomial may

15

arise from the fact that two sub-processes qg and qq with different multiplicity distributions are the dominant contributors to the event topologies under study. It should be noted that the Monte Carlo and data background distributions give no excess for single or double negative binomial fits.
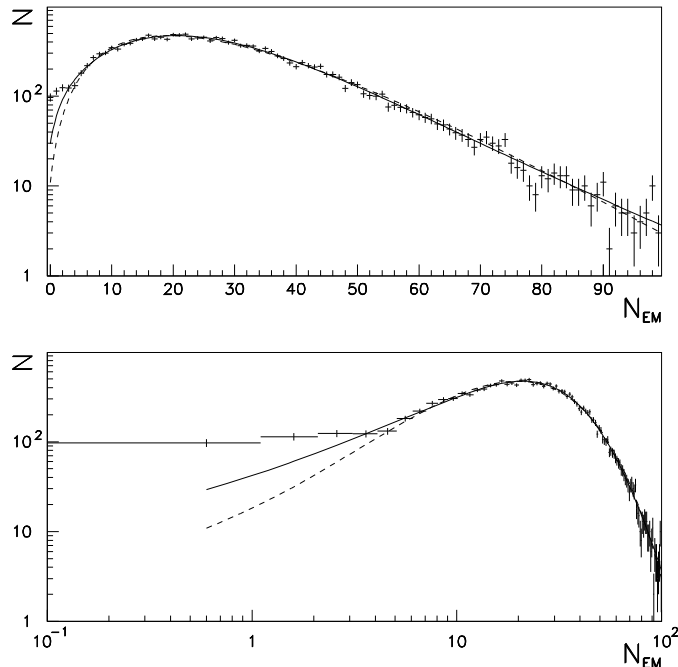

FIG. 13. The preliminary tagged–particle multiplicity distributions obtained from the inclusive event sample for $\Delta\eta_c > 3$. A negative binomial fit to the data for $N_{\rm EM} \geq 4$ and extrapolated to $N_{\rm EM} = 0$ is shown (dashed line) as well as a double negative binomial fit (solid line).

The excess above the fit has been determined by subtracting the fit from the data for $N_{\rm EM} < 4$. A preliminary fractional excess of

$$f = \frac{N(N_{\rm EM} < 4)}{N_{total}} = \left(0.9 - 1.5 \pm 0.1(stat)\right) \times 10^{-2}$$

is obtained where the upper edge of the range comes from the single negative binomial fit and the lower edge of the range is determined using the more conservative double negative binomial fit. The systematic error is currently under study, but it is clear that the largest component of the error is the fitting of the background shape.

To verify that the excess of data above the fit is not caused by a detector effect, the correlation between $N_{\rm EM}$ and the number of tracks observed in the Central Drift Chamber (CDC) [34] is examined for $|\eta| < 1$, where the two detector systems overlap. It is clear from the lego plot shown in Fig. 14 that $N_{\rm EM}$ and the number of tracks seen in the CDC is highly correlated and that there is a significant excess of events in the zero-track/zero-tower bin.
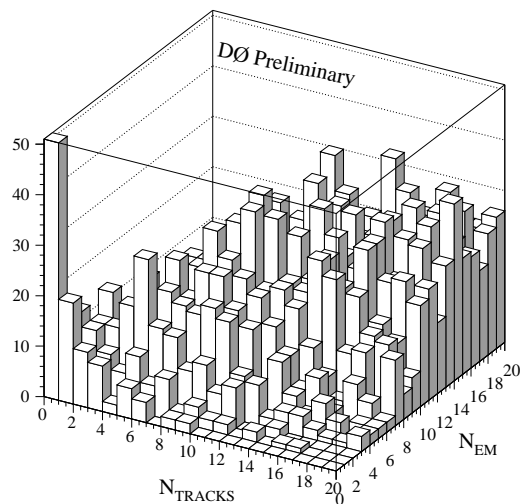
16

FIG. 14. The multiplicity of tracks in the CDC versus the multiplicity of electromagnetic calorimeter towers (N_{EM}).

DØ has previously published [32] the fraction of events which have zero electromagnetic towers ($N_{\mathrm{EM}} = 0$) as a function of $\Delta\eta_c$. This result has been compared to the value of the negative binomial fit for the $N_{\mathrm{EM}} = 0$ bin as shown in Fig. 15. While the fraction of events with $N_{\mathrm{EM}} = 0$ (solid circles) remains constant for $\Delta\eta_c > 2$, the value from the zero bin of the fit (open circles), which represents color-exchange, decreases rapidly. The difference between the two curves could be attributed to the portion of color-singlet exchange events which have no struck calorimeter towers between the jets. This also demonstrates why the upper limit of 1.1% is not inconsistent with the excess of 0.9 —1.5%, as the upper limit only includes rapidity gap events which survive spectator interactions, while the excess above the fit also includes those color-singlet events which have a low multiplicity spectator interaction.
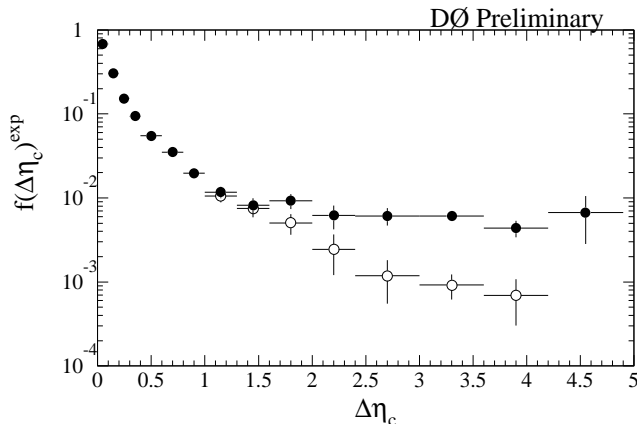

FIG. 15. The fraction of events that have no tagged particles between the two leading jets (solid circles) and the value of the negative binomial fit for the zero multiplicity bin (open circles) as a function of $\Delta\eta_c$. The error bars show the statistical uncertainty only.

D. ZEUS analysis

The ZEUS collaboration has performed a preliminary study of the multiplicity between photoproduction jet events as a function of the separation ($\Delta \eta_c$) between the jet cone edges [35]. Note that this is the inclusive photoproduction jet sample, not the large rapidity gap sub-sample. The clusters of calorimeter energy with $E_T > 200$ MeV between jets of $E_T > 6$ GeV and cone radius $R = 1$ has been measured in bins of $\Delta \eta_c$, and there may be an enhancement at zero multiplicity for the largest $\Delta \eta_c$ bins. In Fig. 16, the rapidity gap fraction is plotted as in Fig. 15. The gap fraction, which shows statistical errors only and has not been corrected for detector effects, plateaus for $\Delta \eta_c > 1.5$, possibly indicating color-singlet exchange in these events, as the color-exchange background should continue to decrease with increasing $\Delta \eta_c$. The plateau of 4% is significantly higher than at the Tevatron, but this could be attributed to a higher survival probability (less rapidity gap events are spoiled by spectator interactions) for the lower center-of-mass ep scattering events.
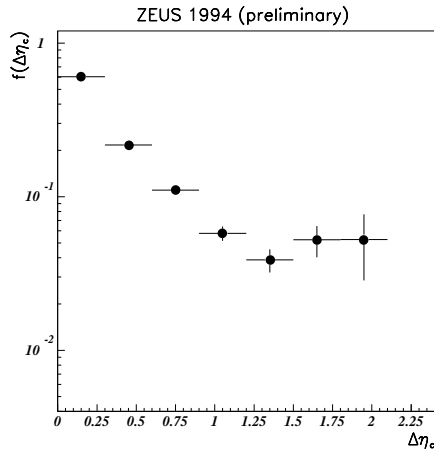

FIG. 16. The rapidity gap fraction (fraction of events with no clusters above threshold) from the ZEUS photoproduction jet sample.

E. Conclusions

Both CDF and DØ have preliminary measurements of the tagged-particle distributions between jets. Both experiments observe a significant excess of events at low tagged multiplicity compared to an assumed background form for the color-octet exchange background. The experiments are consistent within statistical errors and measure an excess of 1–2%, with somewhat different rapidity coverage and jet E_T thresholds. The measured excess for both CDF and DØ is more than ten times larger than predicted excess due to electroweak exchange [36]. The observed excess is consistent with expectations for a strongly interacting color-singlet exchange process, likely indicating observation of a strongly interacting color-singlet. It should be noted that unlike the small momentum transfer ($|t| \sim 0$) processes of Sec. II, the momentum transfer for rapidity gaps between jets is quite significant ($|t| \sim E_T^2$), ranging from 36 GeV^2 at ZEUS to over 1000 GeV^2 at CDF and DØ.

18

IV. CONCLUSIONS

The use of rapidity gaps to tag diffractive events has been quite successful, greatly increasing the scant previous knowledge of the pomeron. The dominantly hard structure of the pomeron indicated by the UA8 Collaboration has been confirmed at HERA. The H1 and ZEUS experiments have gone further, using deep-inelastic scattering to unambiguously demonstrate a quarkonic component of the pomeron, and combining this with cross section results to show evidence for a gluonic component.

CDF has new results on diffractive W and jet production which are putting limits on the pomeron structure and normalization, but as yet no signal has been observed in these channels. More data from CDF and DØ will be forthcoming, as well as new tagged-proton results from ZEUS which will allow measurements of the M_X and t dependence of the pomeron structure.

Evidence for a high-momentum transfer exchange consistent with a strongly interacting color singlet may be showing a different realm of pomeron exchange. Whether or not these exchanges can be attributed to the same pomeron as at low-t remains to be seen. It should be pointed out that all of these studies are indicating the existence of physics outside of current theoretical understanding (and current Monte Carlos) and should therefore be vigorously pursued!

[1] T. Regge, Nuovo Cimento 14 (1959) 951.

[2] P. D. B. Collins, An Introduction to Regge Theory & High Energy Physics, Cambridge University Press (1977).

[3] K. Goulianos, Physics Reports **101** (1983) 169.

[4] A. Donnachie and P.V. Landshoff, Nucl. Phys. **B244** (1984) 322; **B267** (1986) 690.

[5] G. Ingelman and P. Schlein, Phys. Lett. **B152** (1985) 256.

[6] R. Bonino *et al.* (UA8 Collaboration), Phys. Lett. **B211**, 239 (1988).

[7] A. Brandt *et al.* (UA8 Collaboration), Phys. Lett. **B297**, 417 (1992).

[8] A. Brandt *et al.* (UA8 Collaboration), Nucl. Instrum. and Meth. in Phys. Res. **A327** 412 (1993).

[9] ZEUS Collab., M. Derrick et al., Phys. Lett. **B315** (1993) 481.

[10] H1 Collab., T. Ahmed et al., Nucl. Phys. **B429** (1994) 477.

[11] H. Chehime and D. Zeppenfeld, preprint MAD/PH/814 (1994).

[12] POMPYT 1.0: P. Bruni and G. Ingelman (unpublished).

[13] ZEUS Collab., M. Derrick et al., Phys. Lett. **B332** (1994) 228.

[14] ZEUS Collab., M. Derrick et al., Phys. Lett. **B346** (1995) 399.

[15] H1 Collab., T. Ahmed et al., Nucl. Phys. **B435** (1995) 3.

[16] PYTHIA 5.6: H.-U. Bengtsson and T. Sjöstrand, Comp. Phys. Comm. **46** (1987) 43.

[17] ZEUS Collab., M. Derrick et al., DESY 95-115.

[18] ZEUS Collab., M. Derrick et al., Z. Phys. **C65** (1995) 379.

[19] H1 Collab., T. Ahmed et al., Nucl. Phys. **B439** (1995) 471.

[20] H1 Collab., T. Ahmed et al., Phys. Lett. **B348** (1995) 681.

[21] ZEUS Collab., M. Derrick et al., DESY 95-093.

[22] A. Donnachie and P. Landshoff, Nucl. Phys. **B303** (1988) 634.

[23] P. Bruni and G. Ingelman, Phys. Lett. **B311** (1993) 317.

[24] F. Abe *et al.* (CDF Collaboration), Nucl. Inst. and Meth. **A271**, 387 (1988).

[25] P. Melese (CDF Collaboration) *Proceedings of the QCD and High Energy Interaction XXXth Moriond Conference*, Les Arcs, France, March 19-26, 1995.

[26] Y. Dokshitzer, V. Khoze and S. Troyan, *Proc. of the 6th Int. Conf. on Phys. in Collisions* (1986), ed. M. Derrick (World Scientific, Singapore, 1987).

[27] R. S. Fletcher and T. Stelzer, Phys. Rev. **D48**, 5162 (1993).

[28] J. D. Bjorken, Phys. Rev. **D47**, 101 (1992).

[29] V. Del Duca and W. K. Tang, preprint SLAC-PUB-6310 (1993).

[30] I. Dremin, submitted to Physics Uspekhi, FIAN **TD-6**, (1994) and references therein.

[31] E. Gotsman, E. M. Levin and U. Maor, Phys. Lett. **B309**, 199 (1993).

[32] S. Abachi *et al.* (DØ Collaboration), Phys. Rev. Lett. **72**, 2332 (1994).

[33] F. Abe *et al.* (CDF Collaboration), Phys. Rev. Lett. **74**, 855 (1995).

[34] S. Abachi *et al.* (DØ Collaboration), Nucl. Inst. and Meth. **A338**, 185 (1994).

[35] L. Sinclair (ZEUS Collaboration) *Proceedings of the Photon '95 10th International Workshop on Photon-Photon Collisions*, Sheffield, UK, April 1995.

[36] H. Chehime *et al.*, Phys. Lett. **B286**, 397 (1992).